Supporting Information

Friedemann et al. 10.1073/pnas.1009202107

SI Text

I. Experimental Details. For the low-temperature Hall effect and magnetoresistivity measurements, a dilution refrigerator was utilized ($T \geq 18$ mK). A solenoid along with a split-coil magnet allowed for Hall-effect measurements in the crossed-field geometry that is sketched in Fig. S1*a*. In this setup the dual role of the magnetic field is unraveled by using one field (B_1) to generate the Hall response and another field (B_2) to tune the ground state of the sample across the quantum critical point.

The small magnetic field (B_1) provided by the solenoid is used to produce the linear-response Hall effect. Therefore it was oriented along the magnetic hard *c* axis and perpendicular to the electrical current flowing within the crystallographic *ab* plane. Consequently, the Hall voltage V_y is generated transverse to the current within the *ab* plane. The induced voltages were amplified by low-temperature transformers, and the signals were measured by a standard lock-in technique. We extracted the Hall resistivity ρ_H as the antisymmetric component of the field-reversed transversal voltage, $\rho_H(B_1,B_2) = t[V_y(+B_1,B_2) - V_y(-B_1,B_2)]/2I$ (with t being the thickness of the sample). The linear-response Hall coefficient $R_H(B_2)$ was subsequently derived from the initial slope of the Hall resistivity $\rho_H(B_1,B_2)|_{B_2}$

$$R_H(B_2) \equiv \lim_{B_1 \to 0} \rho_H(B_1,B_2)/B_1 \qquad \textbf{[S1]}$$

for small fields $B_1 \leq 0.4$ T (cf. Fig. S2).

The field B_2 that tunes the material from the magnetic ground state to the paramagnetic one is generated by the split-coil magnet and applied within the magnetic *ab* plane. This magnet covers a range of B_2 extending to a value as large as 4 T, nearly 2 orders of magnitude larger than the *ab*-plane critical field, $B_{2c} \approx 0.06$ T. The combination of the two magnets and the dilution refrigerator enabled us to access a wide range of both temperature and magnetic field. This was essential for extracting the temperature dependence of the FWHM as well as for the separation of the crossover and background contributions. The fitting of the isotherms was restricted to below 2 T for the crossed-field Hall results due to deviations from linearity at higher fields. These deviations are likely associated with the Zeeman splitting of the bands, which becomes sizable in this field range since B_2 is applied within the easy magnetic plane.

In the case of the single-field Hall experiment ($B_2 = 0$) (see Fig. S1*b*), the differential Hall coefficient

$$\tilde{R}_H(B_1) \equiv \frac{\partial \rho_H(B_1,0)}{\partial B_1} \qquad \textbf{[S2]}$$

was calculated and analyzed. The fitting of the differential Hall coefficient $\tilde{R}_H(B_1)$ with Eq. **5** of the main text leads to the parameters $\tilde{R}_H^0$ and $\tilde{R}_H^\infty$. In the case of the single-field Hall experiment, the fitting was performed over the full field range up to 4 T.

Special care was spent to a precise alignment of the field B_1 to be parallel to the *c* axis within less than 0.5°. Such precise alignment is essential for the single-field experiment as a small component of this field within the *ab* plane could easily dominate the tuning due to the large magnetic anisotropy of the material.

The magnetoresistivity $\rho(B_2)$ (see Fig. S1*c* for a sketch of the setup) was monitored during the crossed-field Hall-effect measurements. By an analogous fitting with the crossover function, the corresponding parameters ρ^0 and ρ^∞ were extracted. We note that for the magnetoresistivity curves the linear term mB is negligibly small (cf. section IV).

II. Samples. Single crystals of $YbRh_2Si_2$ were synthesized using an indium flux-growth technique as described earlier (1). An additional optimization of the initial composition and the temperature profile led to an improved sample quality. This is manifested in an almost doubled residual resistance ratio of sample 2 (RRR = 120) compared to sample 1 (RRR = 70). All samples were polished to thin ($t \lesssim 80$ μm) platelets and prescreened via resistivity $\rho(T,B)$ measurements to ensure indium-free samples.

Two different samples are considered. Sample 1 was taken from ref. 2 and remeasured in the newly designed high-resolution setup applying the precise alignment procedure described in section IV as a cross-check. Sample 2 was chosen from our highest quality batch. These two samples span the whole range of sample dependences in the low-temperature Hall effect (3): The low-temperature Hall coefficient seems to depend on tiny changes of the composition (samples from the same batch, on the other hand, show identical behavior).

III. Anomalous Hall Contribution. In heavy-fermion metals, an asymmetric scattering of the conduction electrons from the 4*f* moments—the skew scattering—leads to an anomalous contribution to the Hall coefficient mostly relevant at high temperatures (4). However, our analysis of the crossover at the quantum critical point (QCP) is not affected by the anomalous Hall effect, because its contribution to the Hall resistivity

$$\rho_H^a(B_1) = C\rho(B_1)\mu_0 M(B_1) \qquad \textbf{[S3]}$$

is essentially linear in field. It adds a small, but constant anomalous contribution R_H^a to the differential Hall coefficient with an absolute value of less than 0.07×10^{-10} m^3/C. This is negligible compared to the large variation of $\partial\rho_H/\partial B_1$ (compare vertical bars in Figs. S3 and S4*b*). Furthermore, both the inflection point and the sharpness of the crossover are invariant to a constant offset. In Eq. **S3**, C denotes a constant that was determined from fits to $R_H(T)$ at high temperatures (≈100 K in $YbRh_2Si_2$) (5) where no sample dependences are observed (3). The resistivity $\rho(B_1)$ was measured simultaneously, and the magnetization $M(B_1)$ for the relevant geometry ($B \| c$) was taken from ref. 6. Because the anomalous contribution does not influence our analysis, we have simply considered the raw data.

IV. Crossovers in Hall Effect and Magnetoresistivity. Fig. S3 shows the single-field Hall-effect results of $YbRh_2Si_2$ for sample 2. The crossover found in the differential Hall coefficient $\tilde{R}_H(B_1)$ was fitted by the same crossover function as in the crossed-field experiment (Eq. **5** of the main text). In particular, it is possible to identify the crossover and background contributions. The corresponding results and the fits for the crossed-field ($R_H(B_2)$) and the single-field ($\tilde{R}_H(B_1)$) experiments of sample 1 are shown in Fig. S4.

The magnetoresistivity ($\rho(B_2)$) data are illustrated in Fig. S5 for samples 1 and 2. Here, the same crossover function (Eq. **5** of the main text) was used, with the linear term being negligibly small, $m \simeq 0$. We analyzed the magnetoresistivity crossover up to 1 K. This allows us to extract the FWHM over this enlarged temperature range as depicted in Fig. S6 proving that the width

follows the unique linear temperature up to such high temperatures.

No signature is seen in the temperature dependence of the FWHM for any of the experiments at the Néel transition (cf. main text). Only below 30 mK does the FWHM extracted from both the crossed-field Hall effect and the magnetoresistivity crossovers seem to tend slightly toward larger values compared to the overall linear temperature dependence; see Fig. 3 of the main text. We assign this to influences arising from the nearby classical phase transition as at this temperature the phase boundary is approached by the Hall crossover. This is seen in the phase diagram with the FWHM around the crossover field substantially extending into the magnetically ordered phase for temperatures below 30 mK only (cf. horizontal bars in Fig. 4 of the main text), the temperature below which the seeming deviations from linearity occur. Further indications of this additional influence are observed in the crossed-field Hall coefficient curves that exhibit visible spread at lowest temperatures within the ordered phase (Fig. 1 of the main text and Fig. S4).

The FWHM extracted from the single-field measurements, on the other hand, continues to obey the linear form down to the lowest temperatures accessed. Given this continuity, we consider the single-field data to represent the intrinsic quantum critical behavior. This property of the single-field experiment may arise from the fact that only here the tuning field is applied along the magnetic hard axis. For this orientation the magnetization and consequently also the classical magnetic fluctuations are by almost one order of magnitude smaller compared to those for fields applied within the magnetic easy plane (6). The latter configuration is realized in both the crossed-field Hall effect and the magnetoresistivity measurements.

Finally, we note that within the experimental accuracy the FWHM of all the measurements is compatible with the linear form in the whole temperature range. Taking all this together, the data imply that the linear temperature dependence of the FWHM represents the behavior intrinsic to the quantum criticality.

The vanishing FWHM implies a jump of the magnetoresistivity at zero temperature, in contrast to the common behavior of Kondo systems for which the width of the change in magnetoresistivity remains finite at zero temperature (7). This represents a key element in our interpretation of the Hall crossover in terms of a Fermi-surface reconstruction.

V. Sample Dependence of the Background Contribution. The temperature dependences of $R_{\rm H}^0$ and $R_{\rm H}^\infty$ are shown in Fig. 2*A* of the main text for both samples. The results of the low-field value $R_{\rm H}^0$ are in good agreement with those of the measured zero-field ($B_2 = 0$) initial-slope Hall coefficient $R_{\rm H}(T)$ (ref. 3). This is nontrivial as $R_{\rm H}^0$ is the result of the fitting procedure specified in *Materials and Methods* of the main text, and not fixed to the zero-field value. Both $R_{\rm H}^0(T)$ and $R_{\rm H}^\infty(T)$ decrease as the temperature decreases. Below T_N, the initial-slope Hall coefficient clearly obeys a quadratic temperature dependence as demonstrated in Fig. S8*a*. This finding allows for a proper extrapolation of $R_{\rm H}(T)$ and $R_{\rm H}^0(T)$ to $T \to 0$, which in turn enables us to conclude that the difference between $R_{\rm H}^0$ and $R_{\rm H}^\infty$, i.e., the height of the Hall crossover, remains finite for both samples on approaching zero temperature. Identical observations were made for the parameters extracted from the magnetoresistivity crossover (Fig. S8*b* and Fig. 2*B* of the main text) as well as for those of the crossover in the single-field Hall effect (Fig. S7).

The temperature evolution of the parameter m of Eq. **5** of the main text (which describes the linear background) is shown in Fig. S9 for all Hall-effect experiments. The data for the single-field experiments are restricted to below 0.2 K due to the crossover extending over an increasingly large field range with increasing temperature. This prevents a proper determination of the background contribution within the field range of our experiment (cf. Figs. S3 and S4*b*). The crossed-field results of sample 1 are limited to temperatures above 0.065 K due to a lack of high-field data at lower T (cf. Fig. S4*a*).

Taking all these observations together we find a pronounced sample dependence for the quantities describing the background contribution, whereas those associated with the critical crossover are essentially sample independent (cf. main text).

VI. Single-Electron Green's Function and the Hall Crossover. The single-electron Green's function, $G(\mathbf{k},E,T)$ (Eq. **1** of the main text) on either side of the zero-temperature transition and at low temperatures, can be decomposed as

$$G(\mathbf{k},E,T) = G_{\rm coh}(\mathbf{k},E,T) + G_{\rm inc}(\mathbf{k},E,T). \qquad \textbf{[S4]}$$

This decomposition is an immediate consequence of the fact that the phases separated by the QCP are taken to be Fermi liquids. Indeed, because of the jump of the Hall coefficient across the QCP, the Fermi liquids are taken to have large and small Fermi surfaces, respectively. The coherent part of $G(\mathbf{k},E,T)$ is given by

$$G_{\rm coh}(\mathbf{k},E,T) = \frac{z_{\mathbf{k}}}{E - \varepsilon(\mathbf{k}) + i\Gamma_{\mathbf{k}}(T)} \qquad \textbf{[S5]}$$

describing a quasiparticle, and $G_{\rm inc}(\mathbf{k},E,T)$ is a background contribution. The strength of the quasiparticle excitation, $z_{\mathbf{k}}$, formally defined as the residue of the pole, is nonzero in either phase. However, to be compatible with the continuous nature of the zero-temperature transition, $z_{\mathbf{k}}$ must vanish as the QCP is approached: $z_{\mathbf{k}} \to 0$ as $B \to B_c$. At $T = 0$, the quasiparticle damping $\Gamma_{\mathbf{k}}$ vanishes at the small Fermi momenta $\mathbf{k}_{\rm F}$ for $B < B_c$, and at the large Fermi-momenta $\mathbf{k}_{\rm F}^*$ for $B > B_c$; at these respective Fermi momenta, the quasiparticles become infinitely sharp excitations at zero temperature. The coherent part of $G(\mathbf{k},E,T)$ is therefore the diagnostic feature on either side of the transition, and it jumps at the QCP in accord with the sudden Fermi-surface change.

This jump is manifested in the Hall measurement, because the Hall coefficient is independent of the quasiparticle residue. Note that our argument builds on the Landau Fermi-liquid nature of the phases on either side of the QCP, where the Fermi surface and the forms Eqs. **S4** and **S5** are well defined. The Hall coefficient of a Fermi liquid is completely determined by the dispersion of the single-electron excitations near the Fermi surface (8, 9). The fact that the quasiparticle residue does not appear in the Hall coefficient of a Fermi liquid can be seen in a number of related ways. It is known—both phenomenologically (10) and microscopically (11)—that the Boltzmann equation of a Fermi liquid does not depend on the quasiparticle residue; by extension, the Hall coefficient does not depend on the quasiparticle residue. The same conclusion is reached through a study of the Hall coefficient of a Fermi liquid using the Kubo formula (8). Finally, for a spherically symmetric but otherwise arbitrary dispersion, it has been shown explicitly by diagrammatic calculations that the Hall coefficient is not renormalized by the electron-electron interactions (9).

At nonzero temperatures, the quasiparticle relaxation rate at either $\mathbf{k}_{\rm F}$ for $B < B_c$, or $\mathbf{k}_{\rm F}^*$ for $B > B_c$, no longer vanishes. In fact, inside the Fermi-liquid phase (with either large or small Fermi surface), the temperature dependence of $\Gamma_{\mathbf{k}_{\rm F}}$ has to be quadratic in T. However, the Fermi surface remains well defined in these regimes. At finite temperatures, the change from one Fermi surface to the other is therefore restricted to the intermediate quantum critical regime. Because of the absence of a phase transition at any nonzero temperature, the sharp reconstruction of the Fermi surface at $T = 0$ is turned into a Fermi-surface crossover across the $T^*(B)$ line. The restriction to the quantum critical regime implicates that the linear in temperature relaxation rate

present in this regime determines the broadening of the Fermi-surface change. From the relation of the Hall coefficient to the Fermi surface (described above), we associate the width of the Hall crossover with this broadening and consequently with the relaxation rate Γ of the single-electron Green's function.

To be more specific, consider a general scaling form for the single-electron Green's function at the Fermi momentum in the quantum critical region:

$$G(E,T) = \frac{1}{T^{\alpha}}\phi\left(\frac{E}{T^{x}}\right). \qquad \textbf{[S6]}$$

For a Gaussian fixed point, a dangerously irrelevant variable will invalidate E/T scaling and make $x > 1$. Correspondingly, the single-particle relaxation rate Γ (defined in Eq. **4** of the main text) will be superlinear in temperature and the Hall-crossover width as a function of the magnetic field will in general not be linear in temperature. An interacting fixed point, on the other hand, can generate $x = 1$ with a relaxation rate that is linear in temperature and be compatible with the linear-in-T Hall-crossover width observed.

An important question concerns the critical exponent y as defined by the $T^*(B)$ line, $T^*(B) \propto (B - B_c)^y$. This scale equivalently specifies $B^*(T)$, the center of the critical Hall crossover. In general, B^* and FWHM are two independent parameters. Eq. **5**, which fits our data very well (Fig. 1 and Figs. S3–S5), invokes both parameters to characterize the critical component of the Hall crossover. We have already shown that the FWHM is robustly linear in temperature. For the $T^*(B)$ line, Fig. 4 of the main text suggests that the exponent y is less than 1 but its precise determination, especially from the Hall-effect measurements, requires accuracies beyond our present experiments.

1. Trovarelli O, et al. (2000) $YbRh_2Si_2$: Pronounced non-Fermi-liquid effects above a low-lying magnetic phase transition. *Phys Rev Lett* 85:626–629.
2. Paschen S, et al. (2004) Hall effect evolution at a heavy fermion quantum critical point. *Nature* 432:881–885.
3. Friedemann S, et al. (2008) Band-structure and anomalous contributions to the Hall effect of $YbRh_2Si_2$. *Physica B* 403:1251–1253.
4. Fert A, Levy PM (1987) Theory of the Hall effect in heavy-fermion compounds. *Phys Rev B* 36:1907–1916.
5. Paschen S et al. (2005) Anomalous Hall effect in $YbRh_2Si_2$. *Physica B* 359:44–46.
6. Gegenwart P et al. (2002) Magnetic-field induced quantum critical point in $YbRh_2Si_2$. *Phys Rev Lett* 89:056402.
7. Schlottmann, P (1983) Bethe-Ansatz solution of the ground-state of the SU $(2j + 1)$ Kondo (Coqblin-Schrieffer) model: Magnetization, magnetoresistance and universality. *Z Phys B Con Mat* 51:223–235.
8. Kohno H, Yamada, K (1998) A general expression for Hall coefficient based on Fermi liquid theory. *Prog Theor Phys* 80:623–643.
9. Khodas M, Finkel'stein AM (2003) Hall coefficient in an interacting electron gas. *Phys Rev B* 68:155114.
10. Pines D, Nozières P (1999) *The Theory of Quantum Liquids*. New York, Perseus, Vol. I.
11. Betbeder-Matibet O, Nozieres P (1966) Transport equation for quasiparticles in a system of interacting fermions colliding on dilute impurities. *Ann Phys* 37:17–54.

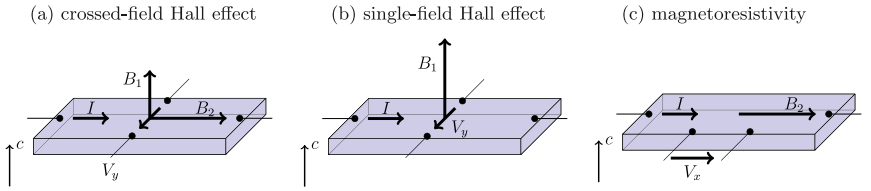

Fig. S1. Experimental setups. The experimental setups of the crossed-field and single-field Hall effect and of the magnetoresistivity measurements are depicted (from left to right).

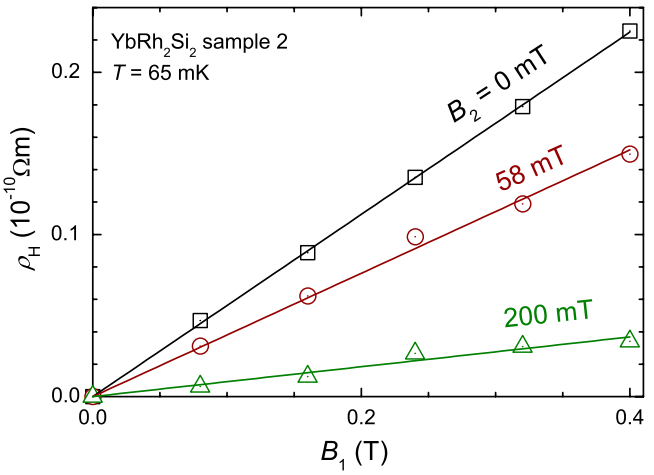

Fig. S2. Determination of the initial-slope Hall coefficient. The figure shows typical isotherms of the Hall resistivity $\rho_H(B_1,B_2)$ at selected fields B_2. The solid lines herein are linear fits to the data used to calculate the linear-response Hall coefficient, $R_H(B_2) = \rho_H(B_1,B_2)/B_1$.

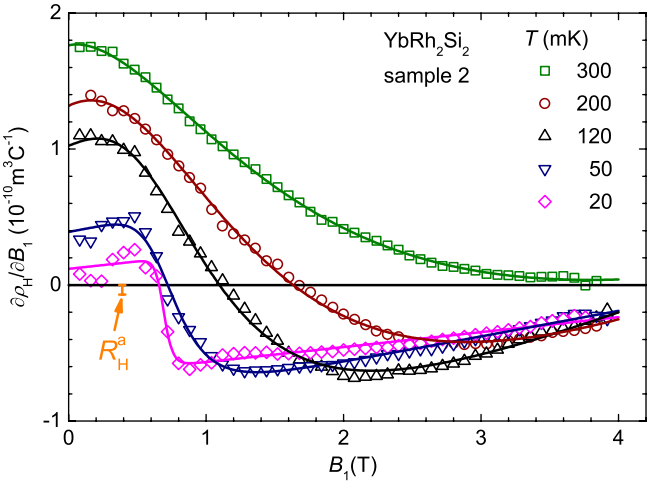

Fig. S3. Single-field results on sample 2 of $YbRh_2Si_2$. Selected isotherms of the numerically derived differential Hall coefficient $\tilde{R}_H(B_1) = \partial\rho_H/\partial B_1$ for sample 2 are plotted against B_1. The solid lines are fits of the crossover function (see *Materials and Methods* of the main text). At large fields $B \gg B_0$, the third term of Eq. **5** of the main text becomes negligible. Consequently, the Hall resistivity is expected to be described by the integral of the first two terms ($\tilde{R}_H^\infty + mB_1$), i.e., $\rho_H = c + \tilde{R}_H^\infty B_1 + \frac{m}{2}B_1^2$ with c denoting the intercept with the ordinate, $\rho_H(B_1 = 0)$. This form was consistently fitted. The vertical, orange bar represents the anomalous contribution determined from Eq. **S3** via the derivative $R_H^a = \partial\rho_H^a/\partial B_1$ (see text).

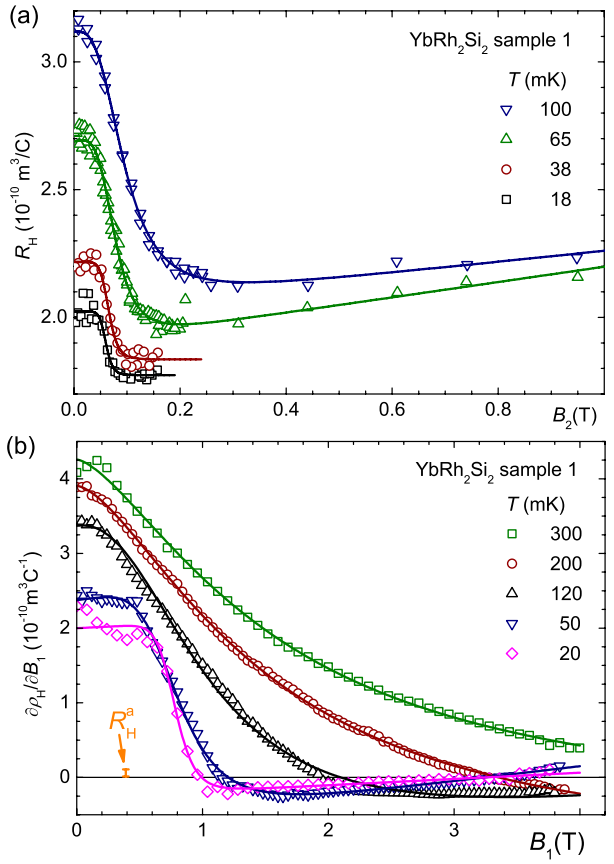

Fig. S4. Hall-effect results on sample 1 of $YbRh_2Si_2$. (*a*) Crossed-field and (*b*) single-field results for the Hall coefficient $R_H(B_2)$ and the differential Hall coefficient $\tilde{R}_H(B_1)$, respectively. For a description of the fitting function we refer to *Materials and Methods* of the main text. As in Fig. S3, the anomalous contribution R_H^a is indicated by the vertical, orange bar (see also section III).

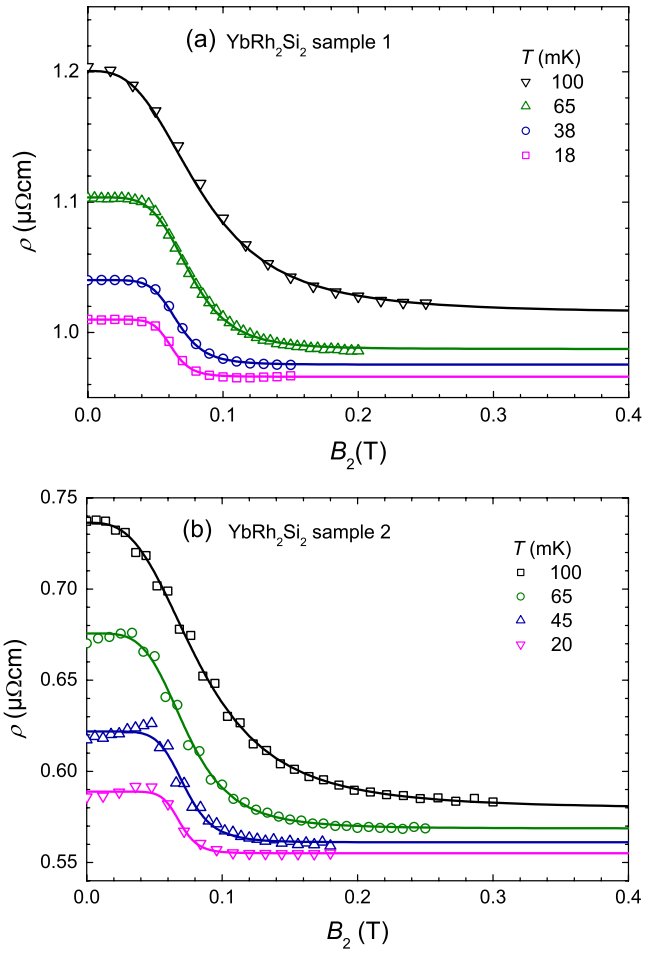

Fig. S5. Crossover in the magnetoresistivity $\rho(B_2)$ of $YbRh_2Si_2$. Results (*a*) for sample 1 and (*b*) for sample 2 are depicted. The data were measured simultaneously with the crossed-field Hall-effect experiment. For the fitting of the crossover (Eq. **5** of the main text), the linear background term was omitted.

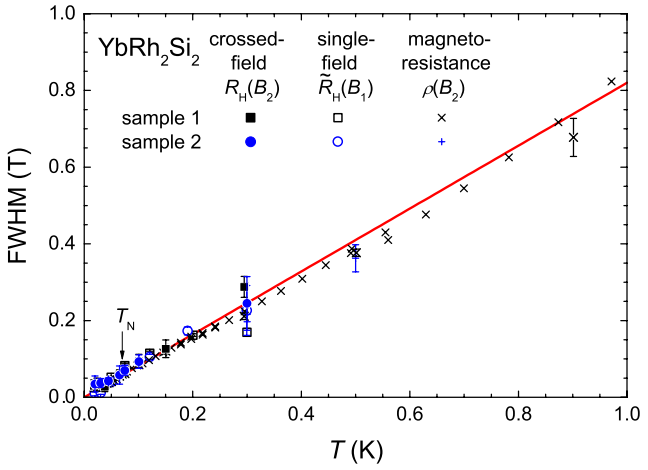

Fig. S6. FWHM up to 1 K. The results extracted from the magnetoresistivity crossover are depicted in an enlarged temperature range up to 1 K. Solid line represents the very same linear fit as in Fig. 3 of the main text. It is referred to Fig. 3 of the main text for further explanations.

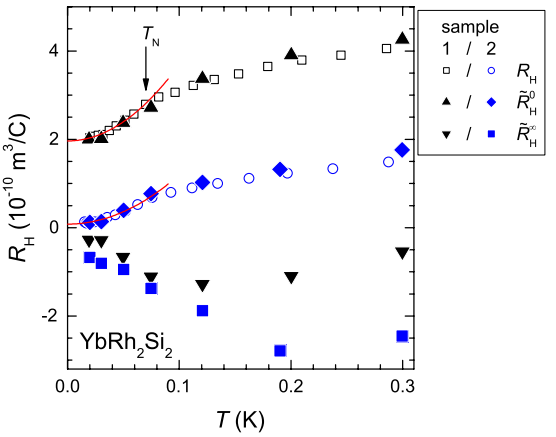

Fig. S7. Limiting values of the single-field Hall crossover. Fit parameters $\tilde{R}_H^0$ and $\tilde{R}_H^\infty$ of the single-field Hall-effect measurement $\tilde{R}_H(B_1)$. Results for sample 1 and sample 2 are depicted along with initial-slope Hall coefficient. Solid curves represent quadratic fits as discussed in the text (see also Fig. S8). Standard deviations are smaller than the symbol size.

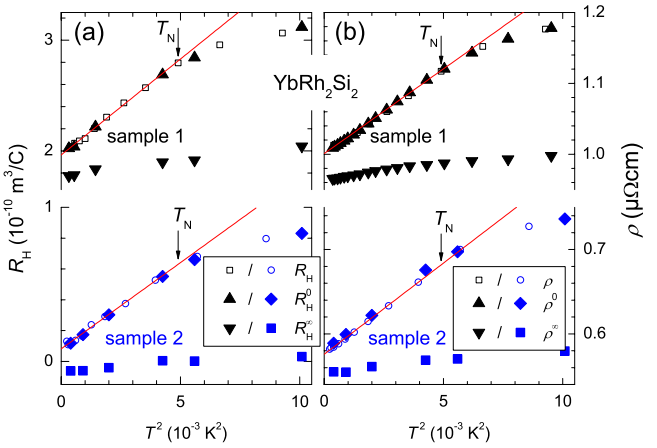

Fig. S8. Evolution of the Hall coefficient in the antiferromagnetically ordered phase. (*a*) Initial-slope Hall coefficient $R_H(T)$ is plotted against T^2 together with the fit parameters R_H^0 and R_H^∞. Solid lines represent fits of the form $R_H(T) = c + A'T^2$ for temperatures below T_N (indicated by arrows) where c denotes the intercept with the ordinate, i.e., the zero-temperature, initial-slope Hall coefficient, $R_H(T = 0)$. These fits are reproduced as solid curves in Fig. 2(*A*) of the main text and in Fig. S7. (*b*) Corresponding plot of the zero-field $\rho(T)$ and the fit parameters ρ^0 and ρ^∞ extracted from the magnetoresistivity crossover with an according fitting function $\rho(T) = \rho_0 + AT^2$ (ρ_0 being the residual resistivity) below T_N, which agrees well with previous observations (6).

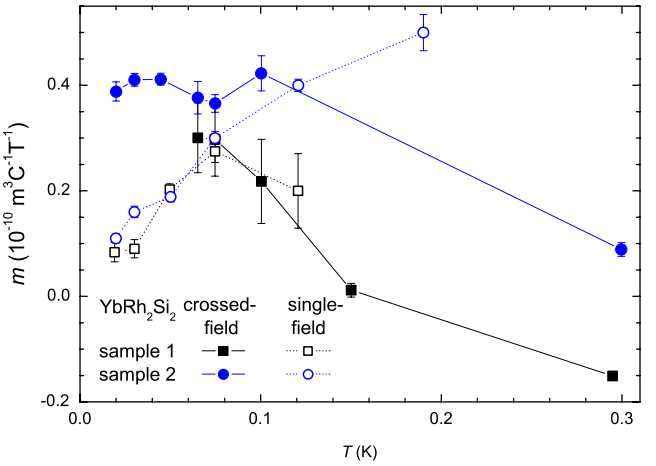

Fig. S9. Temperature dependence of m, the slope of the linear background contribution extracted from the crossed-field and single-field Hall-effect measurements.